Temperature-Induced Nucleation of Poly(*p*-phenylene vinylene-*co*-2,5-dioctyloxy-*m*-phenylene vinylene) Crystallization by HiPco Single-Walled Carbon Nanotubes

S. M. Keogh,*,† T. G. Hedderman,† M. G. Rüther,‡ F. M. Lyng,§ E. Gregan,† G. F. Farrell,† G. Chambers,† and H. J. Byrne†

FOCAS Institute/School of Physics, Dublin Institute of Technology, Kevin St, Dublin 8, Ireland, Materials Ireland, Physics Department, Trinity College Dublin, Dublin 2, Ireland, and Radiation & Environmental Science Centre, FOCAS Institute, Dublin Institute of Technology, Kevin St, Dublin 8, Ireland

Received: November 17, 2004; In Final Form: January 12, 2005

Hybrid systems of the conjugated organic polymer poly(*p*-phenylene vinylene-*co*-2,5-dioctyloxy-*m*-phenylene vinylene)(PmPV) and HiPco single-walled carbon nanatubes (SWNTs) are explored using spectroscopic and thermal techniques to determine specific interactions. Vibrational spectroscopy indicates a weak interaction, and this is further elucidated using differential scanning calorimetry (DSC), confocal laser scanning microscopy, temperature-dependent Raman spectroscopy, and temperature-dependent infrared spectroscopy of the raw materials and the composite. An endothermic transition is observed in the DSC of both the polymer and the 0.1% HiPco composite in the region of 50 °C. Also observed in the DSC of the composite is a double-peaked endotherm at −39 and −49 °C, which does not appear in the polymer. The Raman spectroscopy of the polymer upon increasing the temperature to 60 °C shows a diminished *cis*-vinylene mode at 1575 cm^{-1}, with an increase in relative intensity of the *trans*-vinylene mode at 1630 cm^{-1}. Partially irreversible change in isomerization suggests increased order in the polymer. This change in the polymer is also manifest in the Raman composite spectrum upon increase of the temperature to 60 °C, where the spectrum becomes abruptly dominated by nanotubes. Raman spectroscopy of the composite shows no change at −35 °C; however, infrared absorption measurements suggest that the transition at −35 °C derives from the polymer side chains. Here the composite at −35 °C shows a change in the absorbance of the polymer side chain aryl−oxide linkage at 1250 cm^{-1} and alkyl−oxide stretch at 1050 cm^{-1}. Infrared spectra thus suggest that the transitions in the lower temperature region around −35 °C are side chain-induced, while Raman spectra suggest that the transition at 60 °C is backbone-induced. Furthermore, temperature cycling induces an irreversible decrease in the mean fluorescence intensity of the polymer, coupled with a further reduction in the mean fluorescence intensity of the composite. This suggests that an increase in crystallization of the composite is supported and enhanced by an increase in ordering of the polymer. Implications are discussed.

Introduction

Carbon nanotubes exhibit many unique physical and chemical properties.[1] Raman scattering has been extensively used to explore the relationship between the basic structure and properties of carbon nanotubes, both experimentally[2,3] and theoretically.[4,5] It has been shown that the position and intensity of bands in the Raman spectrum are strongly dependent on the excitation wavelength of the probing laser.[6,7] To gain a greater understanding of the Raman spectra, temperature-dependent measurements of carbon materials, including nanotubes, have been reported.[8−15] Here, frequency shifts have been reported for all peaks in the Raman spectrum. In particular, a linear decrease in the frequency of the radial breathing mode (RBM) and the tangential G band with increasing temperature has been shown.[8−10]

In this paper, temperature-dependent measurements are performed on SWNT composites to further investigate the nature of the interactions in such materials. Much research has been done at ambient temperatures in this area, and initial studies with arc discharge tubes have shown that the organic semi conjugated polymer poly(*p*-phenylene vinylene-*co*-2,5-dioctyloxy-*m*-phenylene-vinylene)(PmPV) allows solubility and even size selective purification of nanotubes as a result of the presence of floppy side chains and conjugation along the polymers backbone.[16,17] This purification process has been extended to nanotubes synthesized by the HiPco process, and it has been shown that this interaction is diameter-dependent rather than tube-type-selective.[18] It is proposed that the PmPV backbone reorganizes into a relatively flat helical structure due to the *m*-phenylene linkage and repulsive interaction between the octyloxy side groups.[19] Panhius et al. have shown that the exposure of the backbone plays an important role in facilitating dipolar binding between the polymer and the nanotube, allowing the polymer to π stack onto the nanotube backbone.[20] The trans linkage is of particular importance in the repeat unit which inhibits polymer aggregation, as all cis conformations have been shown to cause polymer aggregation and inhibit interaction with the nanotube.[17] Coleman et al. have proposed that the polymer is not binding over its entire length but that only a section of it

* Corresponding author. E-mail: Sinead.Keogh@dit.ie.
† FOCAS Institute/School of Physics, Dublin Institute of Technology.
‡ Materials Ireland, Physics Department, Trinity College Dublin.
§ Radiation & Environmental Science Centre, FOCAS Institute, Dublin Institute of Technology.

10.1021/jp044755u CCC: $30.25
Published on Web 03/08/2005

is attached, some 13−14 carbon atoms are binding per molecule.[21] Recent studies have shown that carbon nanotubes nucleate crystallinity in polymers such as polypropylene,[22,23] poly(vinyl alcohol)[24] and poly(*p*-phenylene vinylene-*co*-2,5-dioctyloxy-*m*-phenylene-vinylene)(PmPV).[25] In particular, differential scanning calorimetry (DSC) of these composites has shown an increase in crystallization temperature, arising from the formation of a crystalline layer around the embedded nanotubes.[23,25] Despite extensive research, much remains to be elucidated concerning the nature, and therefore optimization parameters, of the interaction between the composite components. In this study, HiPco/PmPV composites from toluene solution are explored using temperature-dependent (TD)-Raman and TD-FTIR to spectroscopically capture transitions within the DSC. As a decrease in fluorescence intensity is associated with an increase in crystallinity, confocal laser scanning microscopy (CLSM) is employed also to explore changes in fluorescence with respect to temperature of both the polymer and the composite.

Materials Preparation

The HiPco SWNTs (obtained from CNI Houston) (0.1 wt %) were mixed in solutions of PmPV(1 g/L) in toluene. The polymer (1 g/L) was fully dissolved by sonication for 6 h using a low-power (60 W) Branson ultrasonic bath. The composites suspensions were initially sonicated for 20 s using a high-power Branson ultrasonic tip, followed by sonication in a low-power (60 W) sonic bath for 11 h. The composite was left to stand for 48 h, to allow amorphous carbon to precipitate to the bottom. The supernatant was pipetted and degassed for 30 min under a constant flow of nitrogen gas, and thin films were prepared by drop casting onto glass slides. DSC measurements were made using a Perkin-Elmer Pyris Diamond power compensated DSC. The samples; PmPV and 0.1% HiPco/PmPV (∼5 mg) dry composite were placed in closed platinum/iridium crucibles. The samples were cooled first to −100 °C at a rate of 10 °C/min, followed by a heating rate of 40 °C/min to 140 °C. Each sample was run twice to examine the reversibility of observed changes. Heat flow to the sample via the crucible base was measured as a function of temperature.

Mean fluorescence intensity (MFI) measurements of the thin films were taken using a Zeiss LSM 510, confocal laser scanning microscope with a 4× objective lens. Drop-cast films were excited using the argon-ion laser line at 488 nm, and fluorescence was detected using a LP505 filter onto a scan area of 1 mm^2. For infrared measurements, samples were drop cast onto MirrIR slides (Kevley Technologies, Chesterland, Ohio), and spectra were obtained in reflection mode using a Perkin-Elmer Spectrum GX FT-IR microscope. Raman spectra were obtained using an Instruments SA LabRam 1B system. The confocal imaging system uses either a He−Ne laser at 632.8 nm or an argon ion source at 514.5 nm. The laser power was set to ∼1.3 mW at the sample and was focused into a spot size of 1−2 μm in diameter, giving a power density of about 3×10^4 W/cm^{-2}. Each system was fitted with a Linkam LNP cooling stage in order to perform temperature-dependent measurements. The LNP system was used in conjunction with a THMS 600 stage to cool and heat samples as desired. This instrument has a heating and cooling range of −196 to 300 °C, and when water-cooled it is capable of reaching temperatures up to 600 °C. For CLSM, Raman, and FTIR measurements, the sample was cooled to −100 °C and heated at 10 °C/min to +140 °C for two heat cycles. For CLSM measurements, fluorescence images were recorded during heating for every 5 °C and cooling for every 5 °C on the same spot. This system permits time-dependent data acquisiton, which is useful for automated temperature-dependent analysis. Images were recorded every 30 s for 96 min, and sampling time was set to 0.9 s. To aid thermalization, for Raman and IR measurements samples were held for 10 min at each temperature, prior to data acquisition, which was set to 30 s in each case. Spectra were obtained during heating for every 5 °C and cooling for every 10 °C. Raman peak positions were determined by a peak-fitting procedure that uses both Lorentzian and Breit-Wigner-Fano (BWF) functions for semiconducting and metallic modes, respectively.

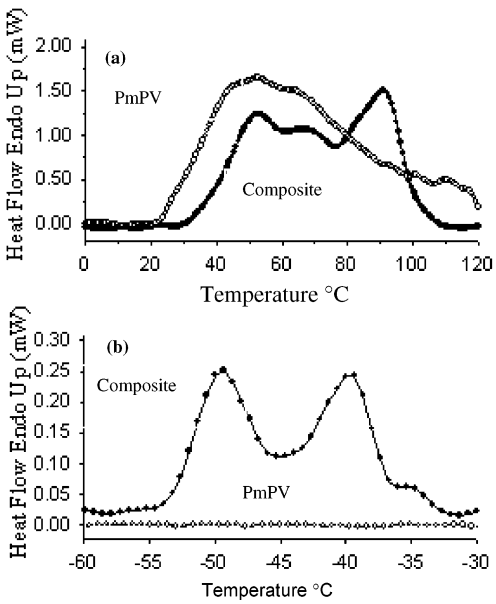

Figure 1. (a) DSC thermograms of the composite and PmPV in the higher temperature regions, and (b) DSC thermograms of the composite and PmPV in the lower temperature regions.

Results and Discussion

DSC has been shown to be a useful tool for the investigation of the effect of carbon nanotubes on the crystallization of polymers.[22−25] This technique has been recently employed in conjunction with thermogravimetric analysis (TGA) and photoluminescence to show that MWNT nucleate PmPV crystallization.[25] Here it was suggested that the nanotubes act as templates upon which the polymer self-assembles. We attempt to reproduce these measurements using SWNT/PmPV composites in the lower temperature regions, and any changes in the DSC should be observable spectroscopically at that temperature. In Figure 1 the first background-corrected differential scanning calorimetry (DSC) cycle is presented for both the PmPV and the SWNT composite and two regions of interest are shown. The DSC of the raw tubes is not presented, but in this temperature region it has been shown that no transitions occur.[26] In Figure 1a it is clear that transitions in the polymer are influencing transitions in the composite. The PmPV film shows a broad endothermic peak at 50.5 °C in the temperature range of 0−130 °C, and this is close to the value of 51 °C presented previously by Ryan et al. for the solution-cast PmPV film.[25] The composite thermogram in Figure 1a, shows an increase in peak temperature to 53 °C, and it is more structured. Shoulders are also present at 72 and 90 °C. Ryan et al. have reported a similar feature at 73 °C in MWNT/PmPV composites and have attributed this to an increased level of ordering of the polymer at the nanotube surface. In the composite the polymer features are still present, but the thermogram is now dominated by a

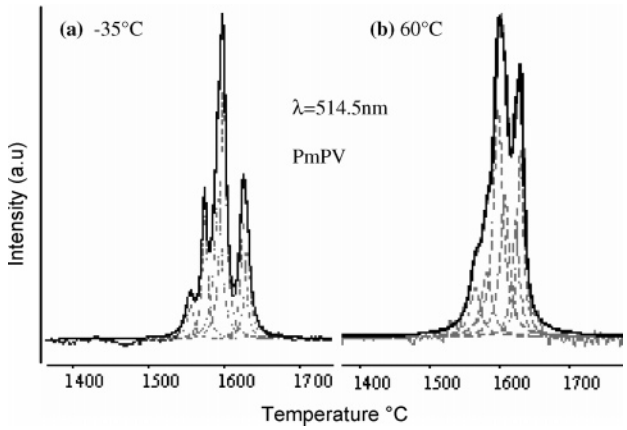

Figure 2. Temperature-dependent Raman for first cycle at excitation wavelength 514.5 nm for (a) PmPV at −35 °C, and (b) PmPV at 60 °C.

feature at ∼90 °C. This shift in the thermogram is attributable to an increased level of ordering of the polymer at the nanotube surface.[25] In Figure 1b a double-peaked endotherm is observed at −49 and −39 °C in the composite spectrum, and its absence in the raw PmPV sample suggests it has origin in the polymer nanotube tube interaction. Changes in the DSC are investigated further using Raman and infrared spectroscopy.

Two procedures in particular have been reported for obtaining temperature-dependent Raman measurements on raw tubes. The first involves varying the incident laser power by laser-induced heating. Here, the temperature is determined in situ by the ratio of the intensity of the Stokes and Anti-Stokes Raman peaks.[8] This technique gives an estimate of the local temperature of the nanotubes which are resonant in the Stokes and Anti-Stokes spectra at a given laser excitation.[15] To avoid induced laser heating of our samples, the power density of the laser was kept low at $\sim 3 \times 10^4$ W/cm^2. Raravikar et al. have reported minimal heating effects at laser power density 3×10^5 W/cm^2.[11] The second procedure involves using an external electric heating device, such as a heating stage.[9] Li et al. have compared both these procedures and have shown that downshifts in the nanotube mode frequencies induced by laser heating are basically identical to those induced by external heating devices.[9] Although the temperature dependence of SWNTs has been well established, here we propose to investigate the temperature dependence of our HiPco/PmPV composite, employing excitation frequencies of 514.5 and 632.8 nm for the raw tubes, the composite, and the pristine polymer. The composite spectra are investigated for any abrupt changes in spectral distribution resulting from alterations in the nature of the polymer−tube interaction.

Before attempting to analyze the thermal behavior of the composites, it is important to understand that of the polymer itself. In Figure 2a,b, the Raman spectrum of PmPV is presented at −35 and 60 °C, respectively. These temperature values were chosen in order to spectroscopically capture the transition in the region of 50 °C in the DSC of the raw polymer. At both temperatures, the PmPV spectrum is dominated by multiple modes around 1600 cm^{-1}, which have been assigned to stretches within the phenyl ring.[27−29] The mode at 1630 cm^{-1} has been assigned to the *trans*-vinylene stretch on the backbone and is common to most PPV-based polymers,[27,30] while the feature at 1577 cm^{-1} is attributed to cis contributions in this polymer.[30] In cycle 1, upon increase in temperature the modes of the PmPV spectrum decrease in intensity due to the inherent temperature dependence of the Stokes spectrum in Raman, although the

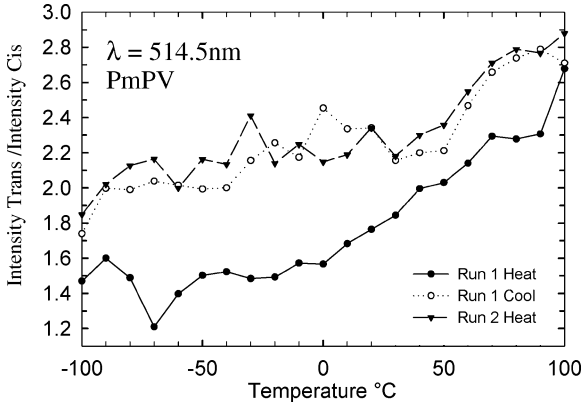

Figure 3. Intensity of trans peak (1630 cm^{-1})/intensity of cis peak (1577 cm^{-1}) for PmPV for Raman excitation wavelength of 514.5 nm

trans-vinylene mode at 1630 cm^{-1} increases in relative intensity, whereas the *cis*-vinylene mode at 1577 cm^{-1} decreases in relative intensity, as shown in Figure 3. Upon cooling, in cycle 1 these modes increase in relative intensity again, although they do not regain their original intensity and are not exact replicas of the same previous temperature spectra. The heating stage of cycle 2 retraces the cooling of cycle 1, indicating that the thermally induced isomerization is essentially complete after the first cycle.

The cis-to-trans ratio has been shown to be a critical parameter affecting the solid-state morphology of the polymer, where increasing the trans content leads to higher backbone ordering of the polymer.[17,20] Figure 3 shows that temperature cycling increases the ratio of trans to cis. As the irreversibility of the DSC is associated with increased crystallinity,[25] spectroscopic analysis indicates that this has origin in a change in the isomerization of the polymer backbone.

Confocal laser scanning microscopy (CLSM) is a useful technique for the investigation of the mean fluorescence intensity (MFI) within samples. The MFI of the PmPV film was measured as a function of temperature and is shown in Figure 4b. In both the first and second run, the MFI of the polymer decreased upon increase in temperature. A reversible, continuous thermally activated loss in fluorescence can be associated, for example, with thermally activated intersystem crossing into triplet levels, lying above the excited state.[31] However the irreversible behavior exhibited in Figure 4 must be associated with changes within the composite. In the first heating cycle, an abrupt decrease in MFI was observed at approximately 60 °C. This abrupt change is still apparent in the second cycle, although not as prominent. The second run also shows a general decrease in MFI, for example in Figure 4a, fluorescence micrographs show run 1 and run 2 at 20 °C where the MFI has been reduced from 56 to 50 a.u, respectively. In conjuction with the DSC and Raman measurements, this decrease in fluorescence intensity may be associated with increased polymer crystallinity. The second cycle of the polymer also shows an abrupt decrease in fluorescence around −40 °C, which is similar to the -first cycle in the DSC of the composite. This suggests that the polymer becomes more crystalline and behaves more like the composite upon temperature cycling.

A decrease in photoluminescence (PL) intensity at ambient temperature has been reported previously for an increase in volume fraction of tubes within the composite.[17,25] Dalton et al. showed that a reduction in photoluminescence along with a change in the spectrum profile was observed as a result of introduction of a specific mass fraction of MWNTs.[17] Ryan et al. suggested that an increase in crystallinity close to the

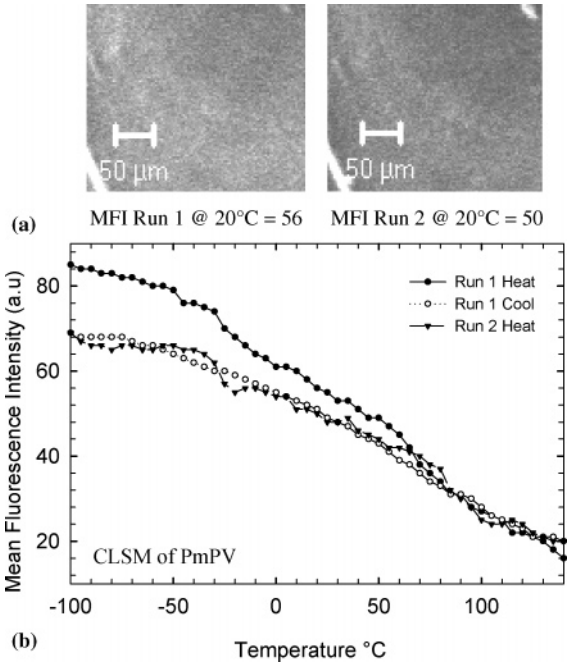

Figure 4. Mean fluorescence intensity measurements using confocal laser scanning microscopy of PmPV for (a) run 1 and run 2 at 20 °C (fluorescence micrographs), (b) as a function of temperature for run 1 and run 2.

nanotube surface can result in a reduction in local PL efficiency.[25] The MFI measurements in Figure 4,b are further evidence of an increase in crytallinity of the polymer and that an abrupt change occurs in the region of 60 °C.

Changes were observed in the region of 60 °C for pristine PmPV using DSC, Raman and CLSM. The irreversibility of the DSC is associated with increased crystallinity. and spectroscopic analysis indicates that this has origin in a change in the isomerization of the polymer backbone. In particular the *trans*-vinylene mode increases in relative intensity compared to the *cis*-vinylene mode, which was shown to decrease. These irreversible changes are also observed using fluorescence microscopy, where a decrease in the MFI in the confocal fluorescence images suggests that temperature cycling induces an increase in crystallinity of the polymer.

Two regions dominate the Raman spectrum of SWNTs. The first originates from the radial breathing of the nanotube between 140 cm^{-1} and 220 cm^{-1}. The second mode, the G line, which is strongly related to the tangential mode in graphite, will only be considered in the following description. Recently it has been shown that, because of nanotube curvature and the folding of the graphite zone into the nanotube zone, the G line contains several modes with different symmetries which are Raman-active, including A_{1g}, E_{1g}, and E_{2g}.[32,33] Polarized Raman studies of individual SWNTs have shown four intrinsic Lorentzian components for the G line of semiconducting tubes, namely, 1549 cm^{-1} [$E_2(E_{2g})$], 1567 cm^{-1} [$A(A_{1g}) + E_1(E_{1g})$], 1590 cm^{-1} [$A(A_{1g}) + E_1(E_{1g})$], and 1607 cm^{-1} [$E_2(E_{2g})$].[34] The Raman spectra for metallic nanotubes in SWNT bundles exhibit only two peaks including a higher-frequency mode which has a Lorentzian line shape at ~1580 cm^{-1} and a lower-frequency mode which exhibits a Breit-Wigner-Fano (BWF) line shape at ~1530 cm^{-1}, although frequency position is wavelength- and sample-dependent.[35,36] The observed Raman spectra using laser excitation of 514.5 nm in Figure 5a and 632.8 nm in Figure 6a are the result of the superposition of both metallic and semiconducting-type nanotubes with different diameters. The

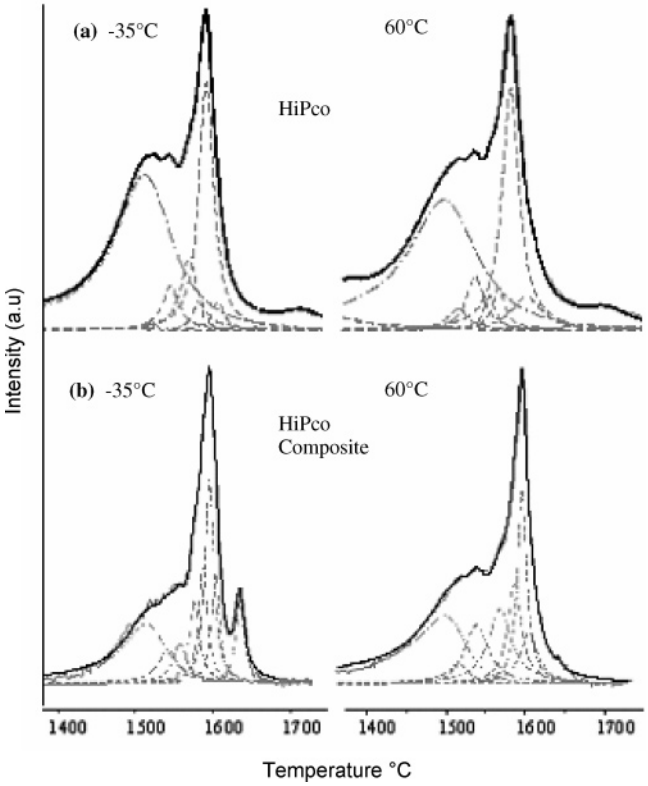

Figure 5. Temperature-dependent Raman at 514.5 nm at −35 and 60 °C for (a) raw HiPco, and (b) 0.1% HiPco composite.

diameter distribution of our raw HiPco sample was obtained by UV/vis/NIR spectroscopy and was found to be 0.73−1.5 nm.[18] This explains the predominantly resonant enhancement of metallic tubes at 514.5 nm and the predominantly resonant enhancement of semiconducting tubes at 632.8 nm, which has been reported previously for HiPco tubes.[37] The high-frequency component of the G line has been fitted using Lorentzian line shapes describing semiconducting tubes.[37] The shape of the lower-frequency BWF metallic mode has been described by the following function; $(I(\omega) = I_o\{1 + (\omega - \omega_o)/q\Gamma\}^2/\{1 + [(\omega - \omega_o)/\Gamma\ ]^2\}$, where I_o, ω_o, Γ, and q are intensity, the BWF peak frequency, broadening parameter, and the asymmetry parameter, respectively.[36]

The spectra presented in Figure 5 are the first run cycle at −35 and 60 °C of (a): G line region of the raw HiPco sample, and (b): the G-line region of the composite at 514.5 nm. The spectra were fitted as specified earlier and are presented in Table 1. Kukovecz et al. have reported seven G-line modes for raw HiPco tubes at an excitation wavelength 514.5 nm.[37] The BWF frequency position in Figure 5 is 7 cm^{-1} lower than their previous reported value of 1522 cm^{-1} (ambient temperature), although the remaining 6 modes are consecutively 3−4 cm^{-1} lower in wavenumber. The fwhm of the BWF mode is considerably larger than the Lorenzian components and is consistent with a high proportion of metallic tubes resonant at this wavelength. The position of the raw HiPco Raman modes in Figure 5a decrease linearly as the temperature is increased, and the behavior is reversible within this temperature range. For temperatures of ~700 K, irreversible changes in the Raman spectrum have been reported as a result of thermal annealing of structural defects in the samples and a burning of the smaller-diameter nanotubes.[15] This downshift has been reported previously for all Raman modes and, in particular, the G-line shift has been attributed to the softening of the C−C bonds.[8−10] The temperature coefficient of Raman frequency shift, $d\omega/dT$ was

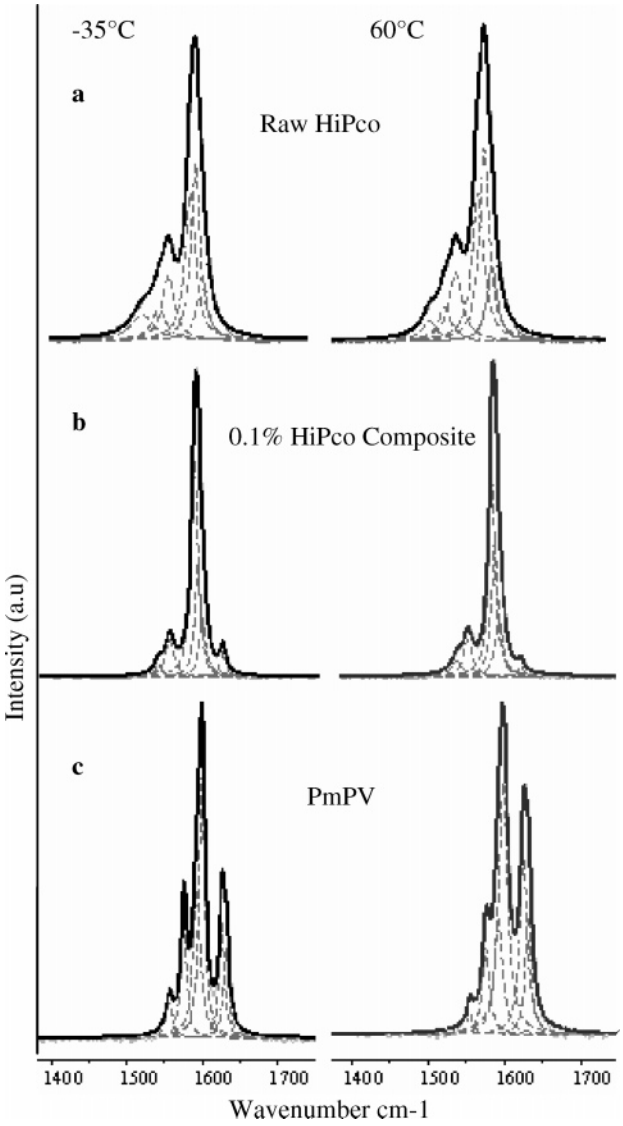

Figure 6. Temperature-dependent Raman at 632.8 nm for (a) raw HiPco, (b) 0.1% HiPco composite, and (c) PmPV.

determined in the temperature range of −100 °C to +100 °C to be $-0.0180\ \mathrm{cm}^{-1}/T$ °C for the highest intensity GM mode at 1590 cm^{-1}, which is close to the previous presented value of $-0.0189\ \mathrm{cm}^{-1}/T$ °C. [11] It has been shown that impurities, defects, and disorder induce elevated coefficients in SWNTs.[9] A general increase in the fwhm was observed as the temperature increased, and this also has been reported previously, although this increase does not have a linear relationship with temperature.[15] There is also a decrease in intensity of the G-line as the temperature increases, and this is attributed to the inherent temperature dependence of Stokes Raman spectrum, which was also observed in the PmPV spectra, as stated previously. Note that in Table 1 the intensities have been normalized to room temperature and are only presented for relative purposes. No abrupt changes were observed in the spectra of the raw HiPco sample, and shifting is reversible.

In Figure 5b, the composite spectra at −35 and 60 °C are presented. The fwhm at each temperature is considerably less than the raw spectrum, and this is indicative of selectivity within the composite as previously reported.[18] Upon increase in temperature, the composite spectrum becomes dominated by nanotubes as the PmPV phenyl modes become overshadowed. The relative intensity of the vinyl mode at 1630 cm^{-1} decreases abruptly around 60 °C and is very weak at 100 °C. The temperature dependence of both the pristine tubes and polymer is smoothly varying in this region; therefore, this abrupt change is characteristic of the composite. Similar changes to the composite spectra were also observed at laser excitation 632.8 nm, as presented in Figure 6b.

Upon increase in temperature the polymer−nanotube binding is significantly altered, and these changes appear to be governed by the change in isomerization to the polymer backbone as seen in the TD-Raman spectra. This change permits an increase in the tangential vibrations of the nanotube backbone. The relative intensity of the BWF mode at 1524 cm^{-1} and the vinyl mode at 1630 cm^{-1} in the composite was graphed as a function of temperature and is presented in Figure 7. It is assumed that only nanotubes contribute to the Raman intensity at 1524 cm^{-1} in the composite, while only the polymer contributes to the Raman intensity at 1630 cm^{-1}. As the temperature is increased above 30 °C, the nanotube signal rises substantially, where at 60 °C the ratio of spectral contribution of tube to polymer is roughly 8:1. This abrupt rise is similar to the transition in the DSC at 60 °C and is interpreted as a dissociation of the polymer backbone from the nanotube, reducing the damping of the nanotubes tangential modes and facilitating a change in isomerization of polymer. Although the relative contributions from the cis and trans modes of the polymer are not discernible in the more complex composite spectrum, upon cooling, the relative intensities do not return to their original positions. This indicates that the nanotube−polymer backbone binding has been altered as a result of heating. This can be translated as an increase in crystallinity of the polymer within the composite as all-trans PmPV has been shown to facilitate polymer−tube

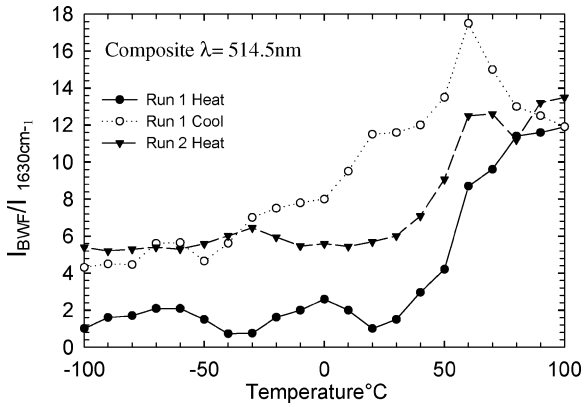

Figure 7. Intensity BWF/intensity 1630 cm^{-1} as a function of temperature for the HiPco composite.

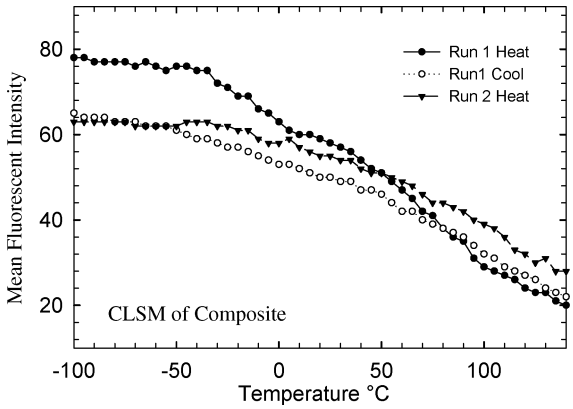

Figure 8. Mean fluorescence intensity measurements using confocal laser scanning microscopy of composite as a function of temperature for run 1 and run 2.

TABLE 1: Frequencies (ω), fwhm ($\Delta\Gamma$), and Relative Intensities (int) of Lorentzian Fitted Modes Associated with Semiconducting Tubes and Breit-Weigner-Fano (BWF) Modes Associated with Metallic Tubes[a] of Raw HiPco, 0.1% HiPco Composite, and PmPV at −35 and 60 °C Excited with Laser 514.5 nm

−35 °C						60 °C					
mode	fitting curve	ω (cm^{-1})	$\Delta\Gamma$ (cm^{-1})	int (a.u)	1/q	mode	fitting curve	ω (cm^{-1})	$\Delta\Gamma$ (cm^{-1})	int (a.u)	1/q
				Raw Hipco							
1	BWF	1516	47	3098	−0.12	1	BWF	1514	50	3033	−0.12
2	Lorentzia n	1523	7	108		2	Lorentzi an	1523	10	144	
3	Lorentzia n	1544	18	897		3	Lorentzi an	1545	18	897	
4	Lorentzia n	1569	24	1461		4	Lorentzi an	1567	26	1461	
5	Lorentzia n	1586	24	1764		5	Lorentzi an	1585	26	1764	
6	Lorentzia n	1591	20	4003		6	Lorentzi an	1588	22	3939	
7	Lorentzia n	1604	19	437		7	Lorentzi an	1608	19	455	
				0.1% HiPco							
1	BWF	1525	34	1776	−0.12	1	BWF	1523	28	2009	−0.12
2	Lorentzia n	1546	27	998		2	Lorentzi an	1531	22	575	
3	Lorentzia n	1559	20	1199		3	Lorentzi an	1547	26	1849	
4	Lorentzia n	1577	15	2514		4	Lorentzi an	1569	27	2337	
5	Lorentzia n	1587	12	3493		5	Lorentzi an	1584	16	3119	
6	Lorentzia n	1594	12	6163		6	Lorentzi an	1591	11	6140	
7	Lorentzia n	1601	11	3317		7	Lorentzi an	1598	20	1562	
8	Lorentzia n	1630	12	2438		8	Lorentzi an	1628	18	231	
				PmPV							
1	Lorentzia n	1555	7	187		1	Lorentzi an	1562	19	39	
2	Lorentzia n	1574	8	423		2	Lorentzi an	1582	18	52	
3	Lorentzia n	1594	13	931		3	Lorentzi an	1598	17	180	
4	Lorentzia n	1600	8	794		4	Lorentzi an	1608	16	113	
5	Lorentzia n	1624	7	500		5	Lorentzi an	1624	13	92	
6	Lorentzia n	1630	9	482		6	Lorentzi an	1631	10	149	

[a] The BWF (parameter 1/q) curves used to fit bands associated with metallic G-modes are −0.12 for raw HiPco and the HiPco composite at both temperatures.

binding, while all-cis conformations cause polymer aggregation which inhibits polymer−tube interaction.[17]

The mean fluorescence intensity (MFI) of the composite was measured and is plotted in Figure 8. In both the first and second run, the MFI of the composite decreased upon increase in temperature, similar to the polymer. Both are plotted on the same scale, and it is noted that in the first heating cycle an abrupt decrease in MFI was observed at −30 °C, which was also observed in the second run of the CLSM of the polymer, although not as prominent, and similar to the transition in the DSC of the composite. A less pronounced decrease at 60 °C was also observed, similar to the Raman spectrum and the DSC. The MFI at −100 °C for the composite in the first cycle and the second cycle is significantly lower than that of the polymer, indicating higher ordering in the composite. This is further evidence that the polymer, which increases in crystallinity due to temperature cycling as shown earlier, is further crystallized upon the introduction of nanotubes. Although there is some evidence of changes in CLSM in the lower temperature regions, TD-Raman showed no abrupt changes; therefore, FTIR was employed to investigate any discontinutities in the lower temperature regions.

TD-FTIR spectroscopy was performed on all samples, and the results are presented in Figure 9. The FTIR spectrum of carbon nanotubes (not shown) agreed with literature.[38] Three main features at 1600, 1400, and 1180 cm^{-1} have been attributed to the C−C and C═C stretching along the hexagonal array of the nanotube backbone.[38] In Figure 9, the composite FTIR spectrum is dominated by the polymer and the nanotube modes within this wavelength range are overshadowed. Strong contributions from the polymers octyloxy side chains are seen. In particular, the aryl−oxide C−O−C stretch between 1230 and 1270 cm^{-1} and the alkyl−oxide stretch between 1020 and 1075 cm^{-1} are observed. The C−H out-of-plane *m*-phenylene ring vibration is found at 778 cm^{-1}.[17] At ambient temperature the

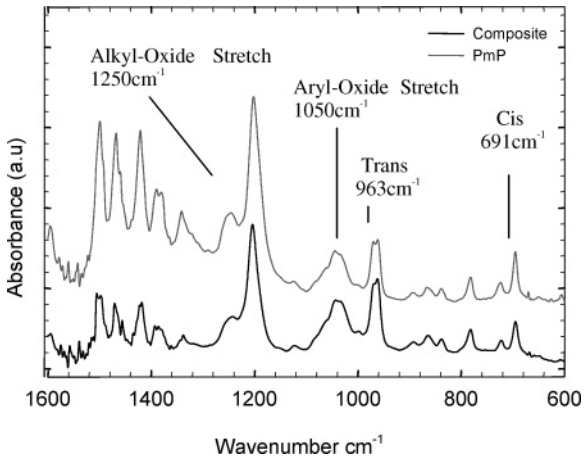

Figure 9. Infrared spectra at ambient temperature for PmPV and the HiPco composite.

infrared spectrum in the low-frequency region shows a typical absorption of the bi-peaked *trans*-vinylene C−H out-of-plane vibration at 970 and 963 cm^{-1}.[17,30] The feature at 691 cm^{-1} is indicative of a *cis*-vinylene unit.[17,30]

Quantative analysis of the cis and/or trans content of the sample can be obtained using the relative peak heights of the absorbance of the 963 cm^{-1} trans mode and 691 cm^{-1} cis mode.[17,30] The relative intensity of the *cis*-vinylene mode in the composite is considerably smaller compared to the polymer, as shown in Figure 10. This shows preferential conformations of trans isomerization of the polymer in the presence of tubes. In the FTIR absorbance spectra of PmPV, the cis-to-trans ratio of the polymer is shown to decrease irreversibily as a function of temperature, similar to Raman. The composite, however, is dominated by the *trans*-vinylene unit and shows an abrupt increase in absorbance at 60 °C, where the ratio of trans to cis is around 4:1.

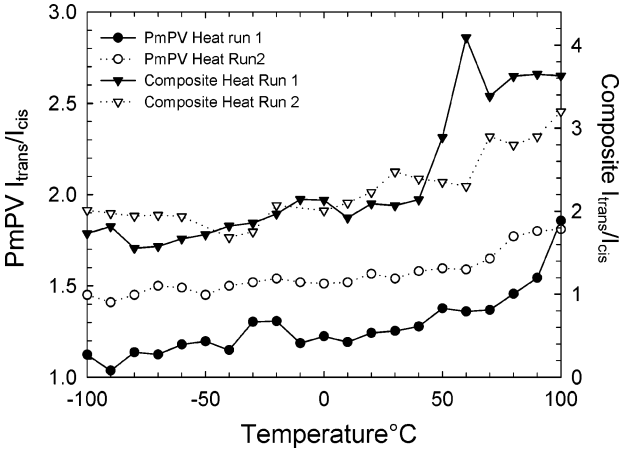

Figure 10. Infrared intensity of trans peak (961 cm^{-1})/intensity of cis peak (693 cm^{-1}) for PmPV and the composite for 2 heating cycles.

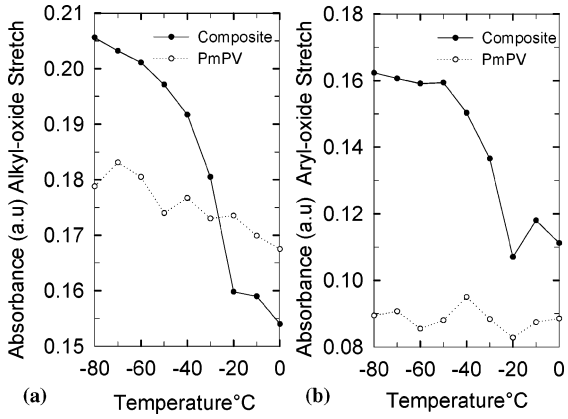

Figure 11. Infrared absorbance of (a) alkyl−oxide stretch and (b) aryl−oxide stretch of both the HiPco composite and PmPV as a function of temperature.

Using Raman and infrared spectroscopy, it has been shown that the transition in the DSC of the composite around 50 °C is due to a change in the nanotube−polymer backbone interaction. To investigate the transitions around −35 °C in the DSC of the composite, the absorbance of the (a) alkyl−oxide stretch and (b) the aryl-oxide stretch was graphed in Figure 11 as a function of temperature. The absorbance of both (a) and (b) in PmPV do not show any discontinuities in the negative temperature region. The composite spectra in both the alkyl−oxide stretch and the aryl−oxide stretch show an abrupt decrease in absorbance around −45 °C, similar to the transition in the composite fluorescent measurements. This observation would seem to indicate possible alterations to the side chain absorption within the composite at this temperature and perhaps is associated with the transition in the DSC and the CLSM at this temperature.

Conclusion

The DSC showed a broad endothermic transition around 60 °C for the polymer. This transition was also observed in the composite, although the peak temperature increases by ∼2 °C, which has been reported previously.[23] Also, a major difference in DSC of the composite is a peak observed at 90 °C. This increase in peak position has been attributed to the polymer self-assembling onto the nanotube backbone, thus increasing the crystallinity of the polymer.[25] Temperature-dependent Raman of the polymer showed a change in the isomerization of the polymer upon increase in temperature. Here the *trans*-vinylene mode at 1630 cm^{-1} increased in relative intensity, whereas the *cis*-vinylene feature at 1577 cm^{-1} decreased in relative intensity. It has been shown previously via experimental and computational techniques that all-trans PmPV, due to its flat helical backbone, facilitates polymer−tube binding, whereas all cis conformations cause polymer aggregation which inhibits polymer−tube interaction.[17] The trans content was shown to increase upon heating, thus increasing its affinity toward binding to the nanotube backbone, as shown in both the Raman and FTIR spectra. Although the relative contributions from the polymer in the Raman are not discernible in the more complex composite spectrum, upon increase in temperature the composite becomes abruptly dominated by nanotubes. At 100 °C, only a very weak contribution from the polymer is observed. This results in an increase in tangential vibration of the nanotube backbone, which is no longer damped. Upon cooling, contributions from the polymer are observed once more; however, the modes do not return to their original positions, showing irreversible changes in the composite. The irreversibility of DSC is associated with increased crystallinity,[25] and spectroscopic analysis shows that this is due to an irreversible change in the isomerization of the polymer backbone. The reduction in MFI in the confocal measurements upon temperature cycling is evidence of a further increase in crystallinity upon introduction of nanotubes.

The DSC also showed a doubly peaked endotherm in the negative temperature region. As no abrupt changes were observed in the Raman spectra at these temperatures, it can be concluded that these endotherms are not backbone-induced. Temperature-dependent infrared was employed to investigate the absorption of the polymers side chain aryl−oxide stretch and alkyl−oxide stretch in the lower temperature regions. FTIR spectra reported previously for MWNT/PMPV composites at ambient temperature in the wavelength range of 600−800 cm^{-1} showed an increase in absorbance of peaks with nanotube content.[39] Here it was suggested that a coherent vibration of adjacent polymer chains causes significant interchain interaction, which is strongly suggestive of an increase in crystallinity on the introduction of nanotubes.[39] An increase in the absorbance of the peaks at 1211 and 1050 cm^{-1} was observed in the composite. Upon heating from the negative temperatures, the absorption of the octyloxy side chains in the composite showed an abrupt decrease in absorbance at about −45 °C, while PmPV showed no significant changes, in the first heating cycle. It has been proposed through atomistic molecular dynamic simulations that the binding energy of the PmPV backbone is 123 kJ/mol per repeat unit and 36 kJ/mol per repeat unit for the octyloxy side chains.[20] It is understood that the higher energy transition in the DSC of the polymer is the melting of the polymer backbone,[25] and the TD-Raman presented earlier in Figure 2c seem to confirm this. Thus, any side-chain-induced transition should occur at a lower temperature in the DSC. This is one possible explanation which would suggest that the doubly peaked endotherm in the DSC is perhaps side-chain-induced. The presence of an abrupt change in the second cycle fluorescence measurement at −40 °C in the polymer might suggest that this transition is related to an induced change in crystallinity of the side chains upon temperature cycling rather than a direct interaction with the nanotubes, although DSC and FTIR first-cycle measurements of the composite would suggest that the transition is induced by the presence of nanotubes. Further work would have to be carried out to confirm whether this transition is intrinsic to the polymer upon temperature cycling and is only accentuated in the composite or whether it is an actual binding of the side chains to the nanotube backbone.

In conclusion, the temperature-induced changes in the Raman spectrum have also been observed in the arc discharge/SWNTs composite at excitation wavelengths 514.5 and 632.8 nm and so are not exclusive to the HiPco composite. An irreversible change in isomerization for PmPV has been shown in both Raman and FTIR. As the FTIR measurements are integrated over a large area (2500 μm^2) in comparison to Raman (2 μm), this confirms that changes are not spot-size-selective. Previous reports have suggested that the nanotube backbone acts as a template upon which the polymer self-assembles, thus increasing crystallinity within the composite.[25] This work supports this statement and further shows that the increased ordering of the polymer backbone, as a result of a change in isomerization, upon heating facilitates increased polymer−tube backbone binding. The irreversible reduction of the MFI in the polymer upon temperature cycling, coupled with a further reduction in MFI in the composite suggests that an increase in crystallinity within the composite is supported and enhanced by an increase in ordering of the polymer. The measurements extend the temperature range of previous work and, in addition to identifying changes in backbone isomerization as the origin of the increased crystallization, also demonstrated changes to the side chain configuration at low temperatures. This is a significant result, because it demonstrates that the optimum polymer−tube interaction does not occur at ambient temperature.

Acknowledgment. The FOCAS Institute is funded under the Program for Research in Third Level Institutions (PRTLI), administered by the HEA. S. M. Keogh acknowledges DIT scholarship support, Trinity College Dublin for PmPV.

References and Notes

(1) Saito, R.; Dresselhaus, G.; Dresselhaus, M. S. *Physical Properties of Carbon Nanotubes*; Imperial College Press: London, 1999.

(2) Pimenta, M. A.; Marucci, A.; Brown, S. D. M.; Matthews, M. J.; Rao, A. M.; Eklund, P. C.; Smalley, R. E.; Dresselhaus, G.; Dresselhaus, M. S. *J. Mater. Res*. **1998**, *13*, 2390.

(3) Jorio, A.; Souza Filho, A. G.; Dresselhaus, M. S.; Swan, A. K.; Unlu, M. S.; Goldberg, B. B.; Pimenta, M. A.; Hafner J. H.; Lieber, C. M.; Saito, R. *Phys. Rev. B* **2002**, *65*, 155412.

(4) Rao, A. M.; Richter, E.; Bandow, S.; Chase, B.; Eklund, P. C.; Williams, K. A.; Fang, S.; Subbaswamy, K. R.; Menon, M.; Thess, R. E.; Dresselhaus, G.; Dresselhaus, M. S. *Science* **1997**, *275*, 187.

(5) Dubay, O.; Kresse, G.; Kuzmany, H. *Phys. Rev. Lett*. **2002**, *88*, 235506.

(6) Jorio, A.; Saito, R.; Hafner, J. H.; Lieber, C. M.; Hunter, M.; McClure, T.; Dresselhaus, G.; Dresselhaus, M. S. *Phys. Rev. Lett*. **2001**, *86*, 1120.

(7) Wang, Y. F.; Cao, W. X.; Hu, S. F.; Liu, Y. Y.; Lan, G. X. *Chem. Phys. Lett*. **2001**, *336*, 47.

(8) Huang, F.; Yue, K. T.; Tan, P.; Zhang, S. L.; Shi, Z.; Zhou, X.; Gu, Z. *J. Appl. Phys.* **1998**, *84*, 4022.

(9) Li, H. D.; Yue, K. T.; Lian, L.; Zhou, L. X.; Zhang, S. L.; Shi, Z. J.; Gu, Z. N.; Liu, B. B.; Yang, R. S.; Yang, H. B.; Zou, G. T.; Zhang, Y.; Iijima, S. *Appl. Phys Lett*. **2000**, *76*, 2053.

(10) Ci, L.; Zhou, Z.; Song, L.; Yan, X.; Liu, D.; Yuan, H.; Gao, Y.; Wang, J.; Liu, L.; Zhou, W.; Wang, G.; Xie, S. *Appl. Phys. Lett.* **2003**, *82*, 3098.

(11) Raravikar, N. R.; Keblinski, P.; Rao, A. M.; Dresselhaus, M. S.; Schadler, L. S.; Ajayan, P. M. *Phys. Rev. B* **2002**, *66*, 235424.

(12) Lliev, M. N.; Litvinchuk, A. P.; Arepalli, S.; Nikolaev, P.; Scott, C. D. *Chem. Phys. Lett.* **2000**, *316*, 217.

(13) Karachevtsev, V. A.; Glamazda, A. Y.; Dettlaff-Weglikowska, U.; Kurnosov, V. S.; Obraztsova, E. D.; Peschanskii, A. V.; Eremenko, V. V.; Roth, S. *Carbon* **2003**, *41*, 1567.

(14) Tan, P. H.; Deng, Y. M.; Zhau, Q. *Phys. Rev. B* **1998**, *58*, 5435.

(15) Corio, P.; Santos, P. S.; Pimenta, M. A.; Dresselhaus, M. S. *Chem. Phys. Lett*. **2002**, *360*, 557.

(16) Dalton, A. B.; Stephan, C.; Coleman, J. N.; Ajayan, P. M.; Lefrant, S.; Bernier, P.; Blau, W. J.; Byrne, H. J. *J. Phys. Chem. B* **2000**, *104*, 10012.

(17) Dalton, A. B.; Coleman, J. N.; Panhuis, M. I. H.; McCarthy, B.; Drury, A.; Blau, W. J.; Paci, B.; Nunzi, J.-N.; Byrne, H. J. *J. Photophys. Photochem. A: Chemistry* **2001**, *5678*, 1.

(18) Keogh, S. M.; Hedderman, T. G.; Gregan, E.; Farrell, G.; Chambers, G.; Byrne, H. J. *J. Phys. Chem. B* **2004**, *108*, 6233.

(19) Panhuis, M. I. H.; Munn, R. W.; Blau, W. J. *Synth. Met.* **2001**, *21*, 1187.

(20) Panhuis, M. I. H.; Maiti, A.; Dalton, A. B.; Van Der Noort, A.; Coleman, J. N.; McCarthy, B.; Blau, W. J. J. *Phys. Chem. B* **2003**, *107*, 478.

(21) Coleman, J. N.; Fleming, A.; Maier, S.; O'Flaherty, S.; Minett, A. I.; Ferreira, M. S.; Hutzler, S.; Blau, W. J. *J. Phys. Chem. B* **2004**, *108*, 3446.

(22) Grady, B. P.; Pompeo, F.; Shambaugh, R. L.; Resasco, D. E. *J. Phys. Chem. B* **2002**, *106*, 5852.

(23) Valentini, L.; Biagiotti, L.; Kenny, J. M.; Santucci, S. *Compos. Sci. Technol*. **2003**, *63*, 1149.

(24) Probst, O.; Moore, E. M.; Resasco, D. E.; Grady, B. P. *Polymer* **2004**, *45*, 443.

(25) Ryan, K. P.; Lipson, S. M.; Drury, A.; Cadek, M., Ruether, M.; O'Flaherty, S. M.; Barrow, V.; McCarthy, B.; Byrne, H. J.; Blau, W. J.; Coleman, J. N. *Chem. Phys. Lett*. **2004**, *391*, 329.

(26) Georgakilas, V.; Voulgaris, D.; Vazquez, E.; Prato, M.; Guldi, D. M.; Kukovecz, A.; Kuzmany, H. *J. Am. Chem. Soc*. **2002**, *124*, 14319.

(27) Orion, I.; Buisson, J. P.; Lefrant, S. *Phys. Rev. B* **1998**, *57*, 4050.

(28) Buisson, J. P.; Lefrant, S.; Mevellec, J. Y.; Orion, I.; Eckhardt, H. *Synth. Met*. **1992**, *49*, 305.

(29) Baitoul, M.; Wery, J.; Buisson, J. P.; Arbuckle, G.; Shah, H.; Lefrant, S.; Hamdoume, H. *Polymer* **2000**, *41*, 6955.

(30) Henderson, K.; MPhil Thesis, Dublin Institute of Technology, Kevin St, Dublin 2, Ireland, 2004.

(31) Wilkinson, F. *Organic Molecular PhotoPhysics*; Birks, J. B., Ed.; Wiley & Sons: Bristol, 1975; p 132.

(32) Kahn, D.; Lu, J. P. *Phys. Rev. B* **1999**, *60*, 6535.

(33) Saito, R.; Takeya, T.; Kimura, T.; Dreselhaus, G.; Dresselhaus, M. S. *Phys. Rev. B* **1998**, *57*, 4145.

(34) Jorio, A.; Dresselhaus, G.; Dresselhaus, M. S.; Souza, M.; Dantas, M. S. S.; Pimenta, M. A.; Rao, A. M.; Saito, R.; Liu, C.; Cheng, H. M. *Phys. Rev. Lett*. **2000**, *85*, 2617.

(35) Pimenta, M. A.; Marucci, A.; Empedocles, S. A.; Bawendi, M. G.; Hanlon, E. B.; Rao, A. M.; Eklund, P. C.; Smalley, R. E.; Dresselhaus, G.; Dresselhaus, M. S. *Phys. Rev. B* **1998**, *58*, 16016.

(36) Brown, S. D. M.; Jorio, A.; Corio, P.; Dresselhaus, M. S.; Dresselhaus, G.; Saito, R.; Kneipp, K. *Phys. Rev. B* **2001**, *63*, 155414.

(37) Kukovecz, A.; Kramberger, Ch.; Georgakilas, V.; Prato, M.; Kuzmany, H. *Euro. Phys. J. B* **2002**, *28*, 223.

(38) Branca, C.; Corsara, C.; Frusteri, F.; Magazu, V.; Mangoine, A.; Migliardo, F.; Wanderlingh, U. *Diamond Relat. Mater*. **2004**, *13*, 1249.

(39) Coleman, J. N.; Ryan, K. P.; Lipson, S. M.; Drury, A.; Cadek, M.; Panhuis, M. I. H.; Wool, R. P.; Barron, V.; Blau, W. J. *Structural and Electronic Properties of Molecular Nanostructures*, XVI International Winterschool on Electronic Properties of Novel Materials; Kuzmany, H., et al., Ed.; 2002; p 557.